Journal of Colloid and Interface Science 601 (2021) 50–59

Contents lists available at ScienceDirect

Journal of Colloid and Interface Science

journal homepage: www.elsevier.com/locate/jcis

Regular Article

Biocatalyst and colorimetric biosensor of carcinoembryonic antigen constructed via chicken egg white-copper phosphate organic/inorganic hybrid nanoflowers

Jiaojiao Gao [a,b], Hui Liu [a,*], Kexin Wu [a], Jifeng Yan [a], Huayu Li [a], Ruixuan Yang [a], Cheng Tong [a], Lingyan Pang [a], Junqi Li [a]

[a] School of Materials Science and Engineering, Shaanxi Key Laboratory of Green Preparation and Functionalization for Inorganic Materials, Shaanxi University of Science and Technology, Xi'an 710021, PR China
[b] College of Chemistry and Chemical Engineering, Yan'an University, Yan'an 716000, PR China

GRAPHICAL ABSTRACT

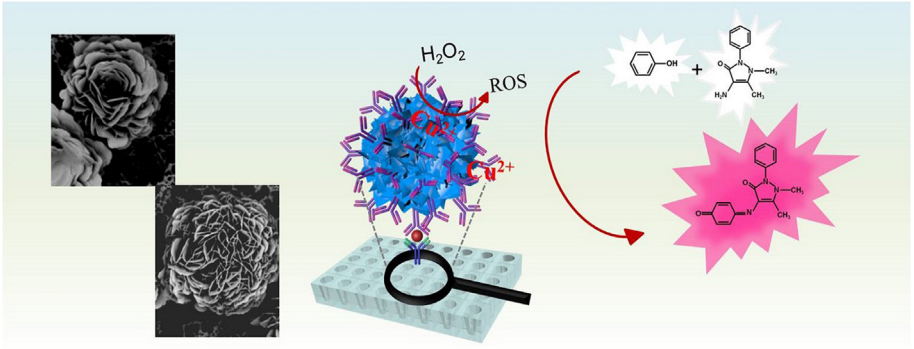

ARTICLE INFO

Article history:
Received 22 January 2021
Revised 12 May 2021
Accepted 13 May 2021
Available online 18 May 2021

Keywords:
Organic/inorganic hybrid nanoflower
Chicken egg white
Colorimetric
Carcinoembryonic antigen
Enzyme-linked immunosorbent assay

ABSTRACT

In this article, the dual-functional chicken egg white-copper phosphate organic-inorganic hybrid nanoflowers (Cu-NFs), combining the functions of signal amplification and biological recognition, were prepared through a simple one-pot method. The Cu-NFs exhibit excellent biocatalytic activity of peroxidase and polyphenol oxidase. Besides, a biotin-labeled secondary antibody encapsulated Cu-NFs-2 (Cu-NFs-2@Biotin-NHS-Ab_2) capture probe was prepared by using the interaction between avidin in the egg white and biotin. Based upon this superiority, the as-prepared Cu-NFs-2 were used in labeled avidin-biotin enzyme-linked immunosorbent assay (Cu-NFs-2 based-LAB-ELISA) to construct a sensitive colorimetric biosensor for the ultrasensitive detection of carcinoembryonic antigen (CEA). Under weak alkaline (pH = 7.5) conditions, the as-developed colorimetric sensor displayed a wide linear range of 0.05–40 ng/mL with a detection limit of 3.52 pg/mL. Furthermore, this colorimetric sensor has been successfully applied to the detection of CEA in human serum samples. Therefore, the as-developed colorimetric sensor has broad application prospects in the field of medical diagnosis and portable detection.

* Corresponding author.
E-mail address: liuhui@sust.edu.cn (H. Liu).

https://doi.org/10.1016/j.jcis.2021.05.069
0021-9797/

1. Introduction

Cancer, a malignant tumor, is one of the major malignant diseases in the world today. According to global reported by the Journal of Clinician Cancer, there were 18.1 million new cases of cancer and 9.6 million deaths from cancer in 2018 [1,2]. Cancer is an important cause of mortality and morbidity in every region of the world, regardless of its level of human development. A lot of studies shown that [3,4] the long-term survival rate of patients with early stage cancer is much higher than that of patients with middle-or end-stage cancer, and the cure rate of some early cancers exceeds 90%. However, the symptoms of early stage cancer are not obvious and are easily overlooked, so that patients miss the best period of treatment. Tumor marker screening technology is an important method for early detection of cancer and it has become the routine item in physical examination [5]. Carcinoembryonic antigen (CEA), serves as a broad-spectrum tumor marker, can reflect the existence of a variety of cancers, and it has great significance in the diagnosis and postoperative monitoring of lung cancer, digestive tract cancer and breast cancer [5–7].

Immunobiosensor, a highly selective biosensor based on antigen-antibody combination, has been widely applied for CEA detection [8]. In order to obtain excellent immunobiosensor, the first problem to be solved is to select an appropriate signal amplification system that can transmit weak immune binding information into an easy-to-read signal. Compared with other signal transduction methods such as fluorescence [9], electrochemistry [10] and electrochemiluminescence [11], colorimetry has attracted more attention from researchers because of its low cost, simple operation, without external instruments and direct signal-obtaining with the naked eye [12,13]. The detection signal of the colorimetric biosensor is derived from the color change caused by the interaction of the analytes. Enzyme-linked immunosorbent assay (ELISA) [14,15] is a traditional colorimetric immunoassay, which uses antigen-antibody specific binding as a recognition unit and the enzyme efficiently catalyzes the color reaction of analytes as a signal amplification unit, thereby achieving the detection of antigen in biological specimens. However, natural enzymes possess the disadvantages of high cost, poor tolerance, easy inactivation and difficulty in recovery, which greatly limits the application and development of the ELISA method in early cancer diagnosis.

With the rapid development of nanoscience and technology, some nanomaterials like Au nanoparticles [16], Fe_3O_4 nanoparticles [17,18] and graphene quantum dots [19] have exhibited simulated peroxidase catalytic performance under specific conditions due to their special physical and chemical properties. These nanomaterials with simulated enzyme properties are called nanoezymes, and show great application potential in ELISA method. Compared with natural enzymes, nanoezymes have the advantages of high catalytic activity, good stability, ability to withstand extreme environments, and high reutilization. However, in practical applications, nanozymes also have some problems such as poor specificity, low antibody labeling efficiency, and their catalytic ability is limited by pH value [17,18]. Generally, the human serum samples must be acidified before using nanozymes to detect CEA. This operation not only complicates the detection process, but also affects the accuracy of the detection results. In recent years, an enzyme-$Cu_3(PO_4)_2$ organic-inorganic hybrid nanoflower, integrating the specificity and high catalytic activity of the enzyme as well as the stability of $Cu_3(PO_4)_2$, has attracted continuous attention from researchers [20,21]. However, this nanoflower has been only used to improve the properties of natural enzymes while the potential applications of the $Cu_3(PO_4)_2$ crystals are rarely explored. According to previous literatures, some copper compounds including $CuFeO_2$ [22], Cu-doped $LaTiO_3$ [23] and Fe/Cu bimetallic particles [24] can be used as Fenton-like reagents to catalyze the decomposition of H_2O_2 to generate active oxygen radicals. Hence these Fenton-like reagents can replace natural peroxidase. It follows that Cu^{2+} in enzyme-$Cu_3(PO_4)_2$ organic-inorganic hybrid nanoflower also has the potential and possibility of peroxidase-like catalysis. Previous studies [25] have demonstrated that Cu^{2+} exists in the enzyme-$Cu_3(PO_4)_2$ organic-inorganic hybrid nanoflower in two forms, one is the $Cu_3(PO_4)_2$ crystals, and the other is coordinated in the protein backbone. Notably, Cu^{2+} coordinated in the protein backbone has a similar chemical structure to the polyphenol oxidase.

Inspired by these research results, we prepared the organic-inorganic hybrid nanoflowers (Cu-NFs) using non-bioactive chicken egg white (CEW) as the organic component and $Cu_3(PO_4)_2$ crystal as the inorganic component. Herein, the CEW plays two roles, one is to act as a protein scaffold to synthesize a flower-like structure of organic-inorganic hybrid nanomaterials and to ensure the existence of two forms of Cu^{2+}, and the other is that the avidin in CEW shows a high affinity for biotin [26]. Thus, the as-prepared Cu-NFs-2 were used as the catalysts and marker Anti-CEA secondary antibodies (Ab_2) labeling materials in combination with an ELISA, in order to construct a colorimetric biosensor for rapid detection of CEA. As shown in the Scheme 1, the Cu^{2+} can catalyze the oxidative coupling of phenol (PhOH) and 4-aminoantipyrine (4-AAP) in the presence of H_2O_2 to produce a pink quinoneimine dye. This chromogenic reaction serves as the signal amplification unit of the colorimetric biosensor. Meanwhile, the biotin-labeled secondary antibody encapsulated Cu-NFs-2 (Cu-NFs-2@Biotin-NHS-Ab_2) capture probes were fabricated due to the interaction between avidin in CEA and biotin. The as-fabricated probes are the recognition unit of the colorimetric biosensor and they can specifically capture CEA. The as-prepared Cu-NFs-2 are used as a biocatalyst for detecting CEA has four advantages as follows: first, a simple one-step synthesis method, the reaction conditions are mild and non-toxic, the synthesis process is simple and does not require complex equipment. Second, the as-prepared Cu-NFs-2 possess excellent biocatalytic activity and specific biological recognition ability. Third, the as-fabricated Cu-NFs-2@Biotin-NHS-Ab_2 capture probe exhibits specificity capture CEA capability. Fourth, human serum samples do not need to be acidified before using the as-developed colorimetric sensor to detect CEA. Therefore, this work developed a colorimetric biosensor based on Cu-NFs-2 labeled avidin-biotin ELISA (Cu-NFs-2 based-LAB-ELISA) for visualization and quantitative detection of CEA in human serum samples.

2. Experimental

2.1. Materials and apparatus

CEW was purchased from a local market and used without further purification. CEA, Anti-CEA monoclonal primary and secondary antibodies (Ab_1 and Ab_2) were supplied by Shanghai Linc-Bio Science Co., Ltd., China. Bovine serum albumin (BSA), 4-AAP, Phosphate buffered saline (PBS, 0.01 M, pH 7.4) and (+)-Biotin *N*-hydroxysuccinimide ester (Biotin-NHS) and were purchased from Shanghai Mackli Biochemical Technology Co., Ltd., China. Human serum was collected from the Second Hospital Affiliated to Xi'an Jiaotong University, China. All other reagents were obtained from Sinopharm Chemical Reagent Co., Ltd., China. All the reagents used in the experiment were of analytical grade. phosphate buffer (PB, 0.1 M) solution was prepared by mixing 0.1 M Na_2HPO_4 and 0.1 M NaH_2PO_4 stock solution. Ultrapure water (18.2 MΩ, Millipore, USA) was used for all experiments.

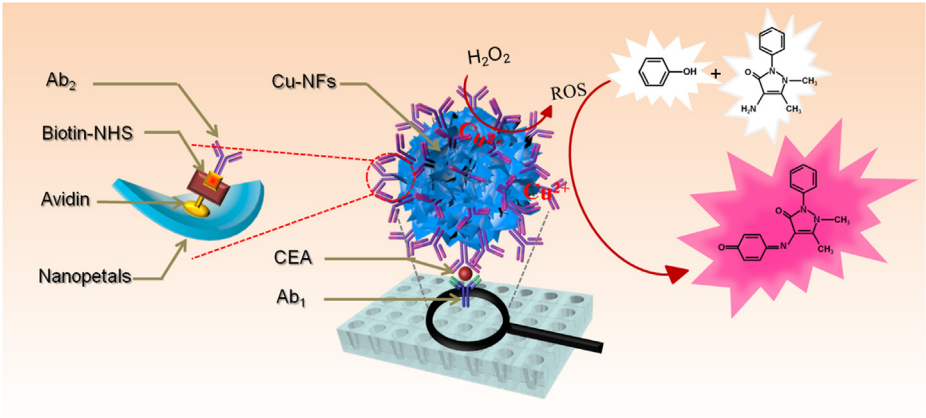

Scheme 1. Schematic illustration of the Cu-NFs-2 based ELISA for CEA detection.

The X-ray diffraction (Rigaku XRD, D/max2200, Japan, Cu Kα 0.154 nm) was used to analyze the crystal structures of Cu-NFs. The microstructure and morphology of the Cu-NFs were investigated by field-emission scanning electron microscope (FE-SEM, Hitachi S-4800) and transmission electronic microscopy (TEM, FEI Tecnai F20). The decomposition process of the CEW during heat treatment was characterized by the thermogravimetric-differential scanning calorimetry (TG-DSC, Netzsch Corporation STA409PC) under N_2 atmosphere in the temperature range of 30–600 °C at a heating rate of 10 °C/min. Fourier-transform infrared (FT-IR) spectra were recorded from sample powder palletized with KBr (sample ratio, 1.5–100 mg) on a Bruker TENSOR27 instrument in the range of 2000–400 cm^{-1}. Surface electronic structure of the Cu-NFs before and after reaction was analyzed by X-ray photoelectron spectroscopy (XPS, ESCALAB 250Xi). Electron spin resonance (ESR) spectra of Cu-NFs were conducted on a Bruker ESP 300E spectrometer.

2.2. Preparation of Cu-NFs

The Cu-NFs was prepared as follows: an aqueous solution of $CuSO_4$ (120 mM, 6 mL) was added into 1 L PB solution (pH 7.0–8.5) containing different concentrations of CEW (2.5 mg/mL, 5 mg/mL, 10 mg/mL, 20 mg/mL and 50 mg/mL, labeled as Cu-NFs-1, Cu-NFs-2, Cu-NFs-3, Cu-NFs-4 and Cu-NFs-5), followed by incubation at 25 °C for 3 days. After incubation, blue precipitates were collected by centrifugation (3500 rpm for 3 min) and the precipitate was washed with ultrapure water and stored in ultrapure water at 4 °C.

2.3. Catalytic activities and steady-state kinetic assay

A typical chromogenic reaction was used to evaluate the catalytic activities and kinetics of Cu-NFs. The chromogenic reaction was performed in solution with 4-AAP, PhOH and H_2O_2 as substrates, and using Cu-NFs as enzyme-like catalyst. The color of the mixed solution changed from colorless to pink during this reaction. The detailed experimental steps are as follows: 5.0 mL PB solution (pH varying from 5.0 to 8.0), 80 μL 4-AAP (50 mM), 80 μL PhOH (50 mM), 80 μL H_2O_2 (0.1 M) and 0.5 mL the catalyst (5 mg/mL, $Cu_3(PO)_4{\cdot}3H_2O$ or the different Cu-NFs) were sequentially added to a 10 mL screw-mouth glass bottle, stirred evenly, and then incubated at room temperature for 30 min. Subsequently, the mixed solution was quickly centrifuged to remove the solid catalyst. Finally, the absorbance changes of the supernatant at 505 nm were recorded using an Agilent Cary 5000 spectrophotometer at room temperature. In order to explore the enzyme-like catalytic mechanism of Cu-NFs-2, the UV–vis absorbance of different reaction systems (System 1# PhOH + 4-AAP, System 2# H_2O_2 + PhOH + 4-AAP, System 3# Cu-NFs-2 + PhOH + 4-AAP, System 4# Cu-NFs-2 + H_2O_2 + PhOH + 4-AAP) was measured.

2.4. Preparation of Cu-NFs-2@Biotin-NHS-Ab_2 capture probes

The Cu-NFs-2@Biotin-NHS-Ab_2 capture probe was obtained by classical LAB method. 2 mg Biotin-NHS was dissolved in 0.1 mL dimethyl sulfoxide (DMSO) and recorded as Solution Ⅰ; 1 mg Ab_2 was dispersed in 0.5 mL borate buffer solution (0.1 M, pH 8.8) and recorded as Solution Ⅱ; 50 mg Cu-NFs-2 were dispersed in 25 mL PBS and recorded as a Suspension Ⅰ; 2.5 μL the Solution Ⅰ was added to the Solution Ⅱ, mixed and incubated at 37 °C for 4 h. 20 μL NH_4Cl (0.1 M) was subsequently added and incubated for 10 min at room temperature. This mixed solution was followed by dialyzing with PBS then the obtained Biotin-NHS-Ab_2 was added to the Suspension I to incubate for 12 h under shaking at 37 °C. Following that, 1 mL 1% BSA solution was added to block the possible remaining active sites. The resulting compounds were washed with PBS and dispersed in PBS then stored at 4 °C. All PBS was autoclaved before use. In order to reduce the damage to the Ab_2 molecules in the test environment, the SEM images of the Cu-NFs-2@Biotin-NHS-Ab_2 capture probes were obtained through a low-voltage Desktop SEM. The surface morphology and microstructureof Cu-NFs-2@Biotin-NHS-Ab_2 was investigated by transmission electronic microscopy (TEM, FEI Tecnai F20) equipped with an energy dispersive X ray spectrometer (EDS).

2.5. Sandwich Cu-NFs-based-LAB ELISA for CEA detection

The colorimetric detection of CEA could be performed with a double-antibody sandwich ELISA method. High concentrations of CEA were diluted with PBS to obtain different concentrations of CEA standards (0.05, 0.5, 5, 10, 20 and 40 ng/mL). The CEA detection experiment was divided into two parts: immunoassay and colour reaction. In the immunoassay, 50 μL Ab_1 (0.02 mg/mL) was attached to the bottom of 96-well plates and incubated for 6 h. Subsequently, 50 μL 1% BSA was used as blocking solution for 1 h to prevent non-specific adsorption. After washing with PBS (to remove unabsorbed Ab_1 and excess BSA), 50 μL of CEA standard with different concentrations were added to the 96-well plates and incubated for 2 h. The unbound CEA was removed by washing with PBS, and then the Cu-NFs-2@Biotin-NHS-Ab_2 capture probe (50 μL, 2 mg/mL) was combined with CEA by immunoreaction for 1 h. The color reaction was performed after washing with PBS to remove unbound Cu-NFs-2@Biotin-NHS-Ab_2 capture probe.

400 μL of System 5# (0.8 mM 4-AAP/0.8 mM PhOH/1.6 mM H_2O_2) mixture was added to a 96-well plate and reacted for 10 min. The color change of the resulting solution was observed with the naked eye and photographed, and then the absorbance (492 nm) of the resulting solution was recorded by Molecular Devices SpectraMax Plus Microplate reader spectrophotometer. The entire experiment was performed in a sterile environment at 37 °C.

3. Results and discussion

3.1. Characterization of Cu-NFs

Here, the unpurified CEW was selected as the organic component to synthesize the organic-inorganic hybrid nanoflower. Compared with other single-component proteins, unpurified CEW has a complex composition, and its main components are ovalbumin, ovalmucin, ovomucin, conalbumin, avidin, and lysozyme [27]. To calculate the isoelectric point (pI) of unpurified CEW, the ZETA potential of CEW in PB solutions with different pH values was measured. It can be seen from Fig. S1 that the ZETA potential of CEW decreases with increasing pH value (the absolute value decreased first and then increased), and its pI is about 5.14. This indicates that the amount of negative charge of CEW increases with increasing of pH when the pH value of the PB solution is greater than 5.14. According to the mechanism of organic-inorganic nanoflower growth reported previously [25], the more negative charge carried by the protein, the more easier of protein coordinate with Cu^{2+}, and more initial nucleation sites of copper phosphate crystals are generated. To further obtain regular-shaped Cu-NFs, the morphology of the Cu-NFs prepared in PB solutions with pH values of 7.0, 7.5, 8.0 and 8.5 was tested by the FE-SEM (Fig. S2). The farther the pH value is from pI, the more regular the morphology of Cu-NFs, the more complete the flower-like structure and the larger the diameter of the flower-like microspheres. At pH = 8.0, complete flower-like microspheres begin to appear, which with uniform particle size and good monodispersity, are self-assembled from a large number of nanopetals with a thickness of about 30 nm.

Subsequently, the morphology and physical properties of Cu-NFs formed at different CEW concentrations were characterized by FE-SEM, TG and BET analysis. As illustrated in Fig. S3, a lot of irregular $Cu_3(PO_4)_2$ nanosheets ($Cu_3(PO_4)_2$ NSs) were observed in the absence of CEW. Fig. 1 shows the FE-SEM images of Cu-NFs prepared at different CEW concentrations. The increase in CEW concentration (i.e., from 2.5, 5, 10, 20 to 50 mg/mL) caused a significant change in the diameter of Cu-NFs (i.e., from 10, 8.5, 7, 6 to 4.5 μm). The higher concentration of CEW can produce more nucleation sites of $Cu_3(PO_4)_2$ crystals, which reduces the diameter of Cu-NFs and makes the structure more compact. The diameter and structure density are the key factors that determine the specific surface area of Cu-NFs. The specific surface area of pure $Cu_3(PO_4)_2$ NSs and Cu-NFs prepared at different CEW concentrations are 19.01, 35.84, 52.72, 34.69, 18.78, and 5.54 m^2/g, respectively (Table S1). Among them, Cu-NFs-2 has the largest specific surface area due to its highly ordered hierarchical flower-like structure. Additionally, the weight percentage of CEW immobilized in Cu-NFs was determined by TG analysis. The TG analysis shows that the weight percentage of CEW in Cu-NFs prepared at different CEW concentrations were 16.11, 21.27, 23.99, 24.43 and 24.62%, respectively. By comprehensive comparison, Cu-NFs-2 (the CEW concentration of 5 mg/mL) has the most complete flower-like morphology and the largest specific surface area.

The chemical composition and structure of as-prepared Cu-NFs-2 have been explored through XRD, FT-IR and XPS measurement. The XRD pattern (Fig. S4a) shows that all the diffraction peaks of Cu-NFs-2 can be well indexed as the $Cu_3(PO_4)_2{\cdot}3H_2O$ (JCPDS 22-0548). Fig. S4b shows the FT-IR spectra of $Cu_3(PO_4)_2$ NSs, CEW and Cu-NFs-2. It can be seen that the FT-IR spectrum of Cu-NFs-2 includes both the typical characteristic absorption bands of CEW and $Cu_3(PO_4)_2$ NSs. The absorption bands at 1159, 1056, 990, 629, and 561 cm^{-1} are attributed to P═O and P—O vibrations [28–30], indicating the presence of phosphate groups. The characteristic absorption bands of CEW were observed at 1649 (amide I) and 1536 cm^{-1} (amide II) [31,32]. Cu2p, P2p, O1s, C1s and N1s core-level XPS spectra of Cu-NFs-2 are shown in Fig. S5. The binding energy peaks of Cu2p (955.6 and 935.7 eV), P2p (133.6 eV) and O1s (531.4 eV) belong to Cu^{2+} and PO_4^{3-} [33–36]. The peaks of C1s and N1s at the binding energy of 284.6, 285.8, 287.9, 399.6 and 400.1 eV are derived from CEW [37–39]. Compared with that of $Cu_3(PO_4)_2$ NSs (Fig. S6), the peaks of $Cu2p_{1/2}$ and $Cu2p_{3/2}$ belong to Cu-NFs-2 shifted toward the high binding energy by approximately 0.53 and 0.64 eV, respectively. This indicates that a new coordination bond is formed between Cu^{2+} and CEW framework [40]. Based on the above results, Cu-NFs-2 was confirmed to be composed of CEW and $Cu_3(PO_4)_2{\cdot}3H_2O$, and a new chemical bond was formed between CEW and $Cu_3(PO_4)_2{\cdot}3H_2O$.

3.2. Catalytic activities and kinetics of Cu-NFs

In this study, the H_2O_2 + PhOH + 4-AAP system was used to evaluate the catalytic activities and kinetics of the as-prepared Cu-NFs. It is known that in the presence of H_2O_2, PhOH and 4-AAP can undergo a coupling reaction to produce a pink quinoneimine dye [41,42]. As shown in Fig. S7, the reaction product has the largest absorption at wave length of 505 nm. This indicates that the reaction product is the result of the coupling of phenol and 4-AAP, rather than the product of the catalytic oxidation of phenol or 4-AAP alone. However, this coupling reaction proceeds very slowly in the absence of a catalyst. Therefore, the as-prepared Cu-NFs were used as a catalyst to catalyze the above coupling reaction. Fig. 2a shows the UV absorbance and photograph in sunlight of different reaction systems. In the absence of Cu-NFs-2 and H_2O_2, no obvious color variation of the System 1# was observed, and its absorbance is close to zero. For the addition of H_2O_2 alone into the System 1#, the color of System 2# appeared extremely light pink colour, and its absorbance increased slightly. The addition of Cu-NFs-2 HNFs further darkened the pink colour of System 3#, meanwhile, increased the absorbance of System 3#. This proves that Cu-NFs-2 possesses the mimic polyphenol oxidase catalytic activity. The simultaneous addition of H_2O_2 and Cu-NFs-2 to the System 1# caused a significant increase of the absorbance of System 4#, and the color of the System 4# was darker than that of other Systems. This indicates that Cu-NFs-2 can catalyze the decomposition of H_2O_2, thereby accelerating the coupling reaction. In general, the pH value of the reaction system is an important factor affecting the catalytic activity of Cu-NFs-2. Fig. 2b shows the UV absorbance and photograph in sunlight of System 4# at different pH values from 5.0 to 8.0. Like natural enzymes, the catalytic activity of Cu-NFs-2 also depends on pH values. It can be seen that the catalytic activity of Cu-NFs-2 increases significantly with the increase of pH value, and then tends to stabilize when the pH value reaches 7.5. Fig. 2c displays the absorbance along time for System 2# with different catalysts (without catalyst, $Cu_3(PO_4)_2$ NSs and Cu-NFs-2). Without the addition of catalyst, there was no obvious color variation in System 2# and its absorbance increased slightly after 45 min. It is difficult for PhOH to react with 4-AAP only through H_2O_2 catalysis. For System 2# with catalyst, the Cu-NFs-2 catalytic system reaches the reaction platform in 30 min, and its reaction rate is much faster than that of the $Cu_3(PO_4)_2$ NSs catalytic system. The color variations of the System 2# with different catalysts were observed, as shown in the inset of Fig. 2c. The colors of Cu-NFs-2/System 2#, $Cu_3(PO_4)_2$ NSs/System 2# and System 2#

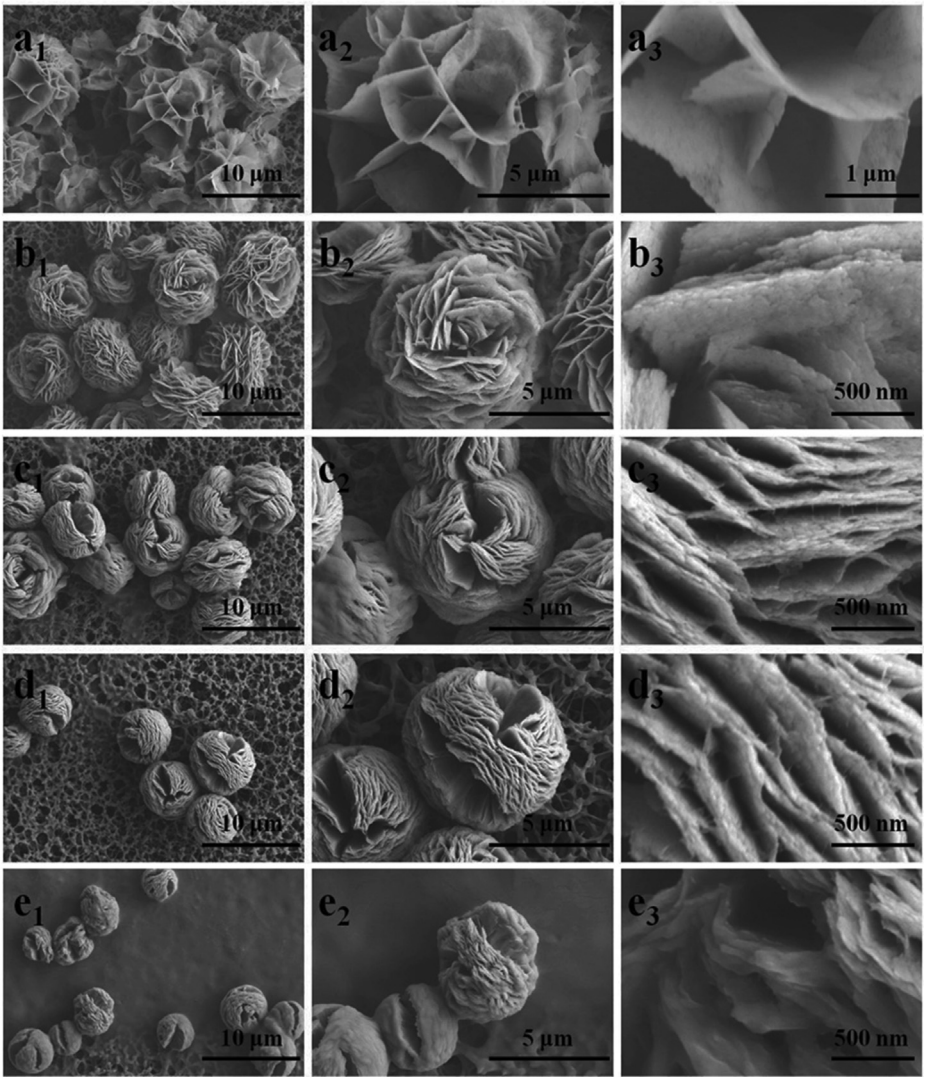

Fig. 1. FE-SEM images of the Cu-NFs formed under different CEW concentrations. ($a_{1\text{-}3}$) 2.5 mg/mL; ($b_{1\text{-}3}$) 5 mg/mL; ($c_{1\text{-}3}$) 10 mg/mL; ($d_{1\text{-}3}$) 20 mg/mL; ($e_{1\text{-}3}$) 50 mg/mL; other conditions: 120 mM Cu^{2+}, 0.1 M PB solution at pH 8.0, reaction at 25 °C for 72 h.

are pink, light pink and colorless, respectively. Furthermore, -ln I_{sub} (I_{sub} is the value obtained by subtracting the real-time absorbance from the saturated one) [43] was calculated to obtain an approximate linear relationship between -ln I_{sub} and the reaction time, as shown in Fig. 2d. The reaction of this system followed pseudo-first-order kinetics. By calculating this linear relationship, the average reaction rate constants (k) of Cu-NFs-2/System 2# (12.43×10^{-2} min^{-1}) is about five times that of $Cu_3(PO_4)_2$ NSs/System $2^{\#}$ (2.46×10^{-2}). Subsequently, the catalytic activity of Cu-NFs prepared at different CEW concentrations was further explored. As shown in Fig. 2e, the Cu-NFs-2 first reached the reaction platform, indicating that it possesses the best catalytic performance. Compared with other Cu-NFs/System $2^{\#}$, the Cu-NFs-2/System $2^{\#}$ shows the darkest pink (inset of Fig. 2e). The -ln I_{sub}-time fitting curve (Fig. 2f) was used to further estimate the average reaction rate constants (k) of the five Cu-NFs catalyst systems as 3.74×10^{-2}, 12.43×10^{-2}, 2.30×10^{-2}, 2.13×10^{-2} and 0.89×10^{-2} min^{-1}, respectively. The catalytic performance of Cu-NFs-2 is significantly better than other Cu-NFs and $Cu_3(PO_4)_2$ NSs, which could be attributed to its larger specific surface area. Therefore, Cu-NFs-2 was used as a catalyst in subsequent experiments unless otherwise specified.

3.3. Enzyme-like catalytic mechanism of Cu-NFs-2

According to the above experimental results, it can be concluded that Cu-NFs-2 has the catalytic activity like that of mimic peroxidase and polyphenol oxidase simultaneously under weak alkaline conditions. And the mimic peroxidase plays a leading role in the H_2O_2 + PhOH + 4-AAP reaction system. To clarify the catalytic mechanism of Cu-NFs-2 in simulating peroxidase, the electron spin resonance (ESR) spectroscopy was employed to test the catalytic decomposition of H_2O_2 by Cu-NFs-2. Fig. 3a shows ESR spectra obtained after 3 min incubation of Cu-NFs-2 and H_2O_2 in PB solution containing 5,5-dimethyll-pyrroline *N*-oxide (DMPO). The characteristic peaks of hydroperoxyl radical ($HO_2^{\bullet}$), superoxide anion radicals ($O_2^{\bullet-}$) and hydroxyl radicals (•OH) are clearly observed [44–47], which confirms the Cu-NFs-2 can catalyze the decomposition of H_2O_2 to generate reactive oxygen radicals (ROS) in PB solution (pH = 7.5). This indicates that the as-prepared Cu-NFs-2 has the mimic peroxidase catalytic activity. Subsequently, the catalytic activity of Cu-NFs-2 in mimic polyphenol oxidase was studied by measuring the UV–vis absorption spectrum of System $3^{\#}$. As shown in Fig. S8, an absorption peak at 505 nm of the System $3^{\#}$ was observed in the UV–vis absorption

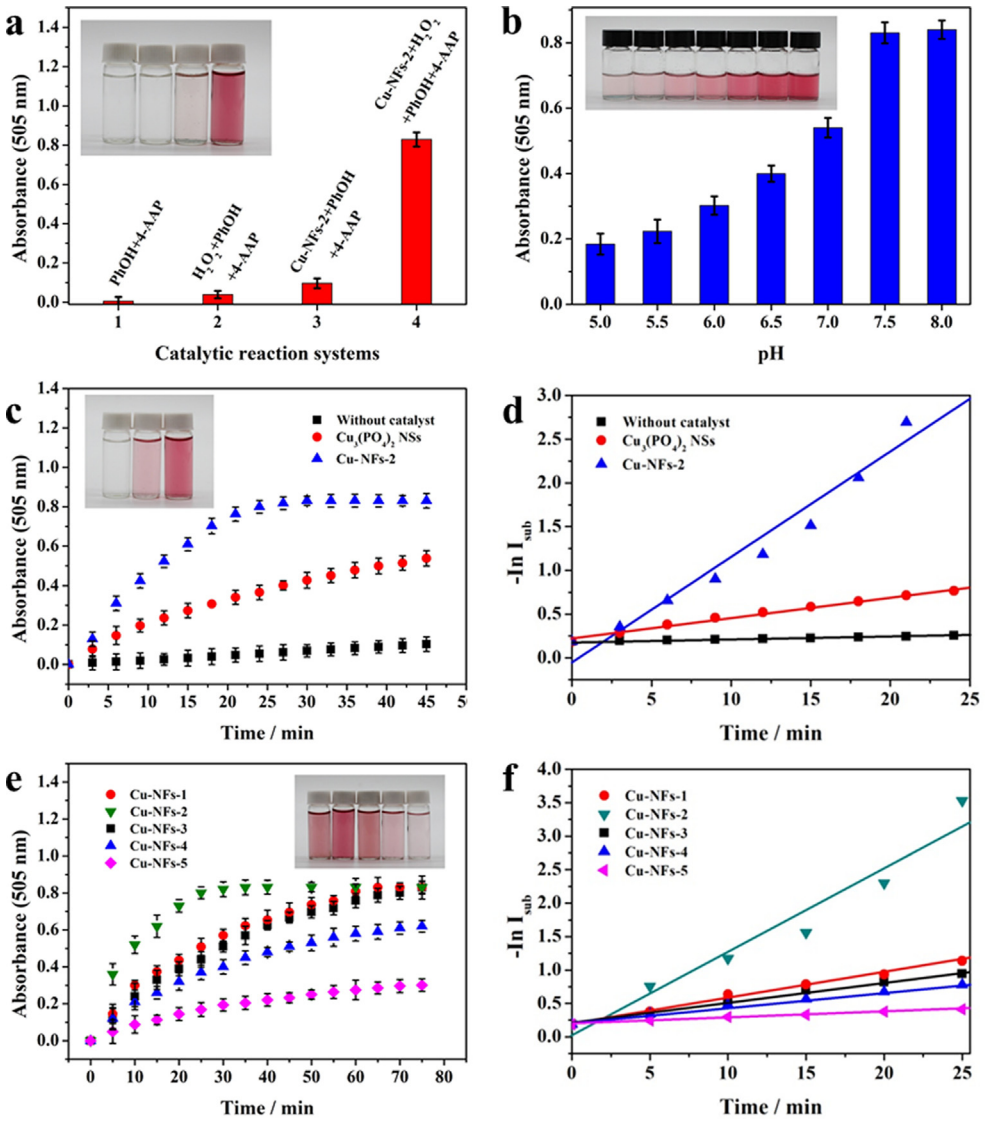

Fig. 2. (a) UV–vis absorbance (λ_{ab} = 505 nm) of different reaction systems; inset: photograph in sunlight of different reaction systems (System 1# PhOH + 4-AAP, System 2# H_2O_2 + PhOH + 4-AAP, System 3# Cu-NFs-2 + PhOH + 4-AAP, System 4# Cu-NFs-2 + H_2O_2 + PhOH + 4-AAP), the reaction systems were stirred and incubated for 30 min (n = 5, n is defined as the times of repeat experiments). (b) UV–vis absorbance (λ_{ab} = 505 nm) of the System 4# in 0.1 M PB solution with different pH values from 5.0, 5.5, 6.0, 6.5, 7.0, 7.5 to 8.0; inset: photograph in sunlight of System 4# in 0.1 M PBS with different pH values, the reaction systems were stirred and incubated for 30 min (n = 5). (c) Catalytic kinetics of three reaction systems; inset: photograph in sunlight of three reaction systems ([H_2O_2 + PhOH + 4-AAP], [$Cu_3(PO_4)_2$ + H_2O_2 + PhOH + 4-AAP] and [Cu-NFs-2 + H_2O_2 + PhOH + 4-AAP]) (n = 3). (d) Plots of -ln I_{sub} vs time for three reaction systems. (e) Catalytic kinetics of System 4# in the presence of different Cu-NFs; inset: photograph in sunlight of System 4# in the presence of different Cu-NFs (n = 3). (f) Plots of -ln I_{sub} vs time for System 4# in the presence of different Cu-NFs. Experimental conditions: room temperature, 0.5 mg/mL catalyst, 0.8 mM 4-AAP, 0.8 mM PhOH, and 1.6 mM H_2O_2 in 0.1 M PB solution for each system.

spectrum a. This proves that Cu-NFs-2 possesses the mimic polyphenol oxidase catalytic activity. For comparison, $Cu_3(PO_4)_2$ NSs were also used to catalyze the reaction of System 1#. No obvious absorption peak is found in the UV–vis absorption spectrum b. This verifies that the mimic polyphenol oxidase catalytic activity of Cu-NFs-2 is mainly derived from the Cu^{2+} coordinated to the protein, rather than the Cu^{2+} in the inorganic component of $Cu_3(PO_4)_2$ crystal.

To further explore the role of Cu-NFs-2 in the reaction of System 4#, the precipitate of Cu-NFs-2 after the reaction was collected and washed. From the photograph in sunlight of Cu-NFs-2 before and after the reaction of System 4# (inset of Fig. 3b), it can be clearly observed that the colour of Cu-NFs-2 precipitates changed from initial blue to green. Subsequently, the valence changes of the copper ions on the surface of Cu-NFs-2 before and after the reaction of System 4# was analyzed by XPS. Fig. 3b shows the XPS spectra of $Cu2p_{3/2}$ core level of Cu-NFs-2 before and after the reaction of System 4#. For $Cu2p_{3/2}$ XPS spectrum (after reaction) of Cu-NFs-2, it can be observed that two peaks of Cu^{2+} are located at binding energies of 935.7 and 935.0 eV, respectively, a peak of Cu^{+} is located at binding energy of 932.8 eV. Compared with that of the Cu-NFs-2 before reaction, in which the peaks of Cu^{2+} is located at the binding energies of 935.7 eV, the second peak for the Cu-NFs-2 after reaction were shifted toward lower binding energy regions by amounts of 0.7 eV. This suggests that the Cu^{2+} on the surface of Cu-NFs-2 in the reaction of System 4# gained electrons and was reduced, and it is also accompanied by the formation of Cu^{+}. The results of ESR and XPS confirm that the Cu^{2+} on the surface of Cu-NFs-2 can catalyze the decomposition of H_2O_2, and the catalytic mechanism is postulated as follows: [23,44–48]

$$Cu^{2+} + H_2O_2 \rightarrow Cu^{+} + HO_2^{\cdot} + H^{+} \quad (1)$$

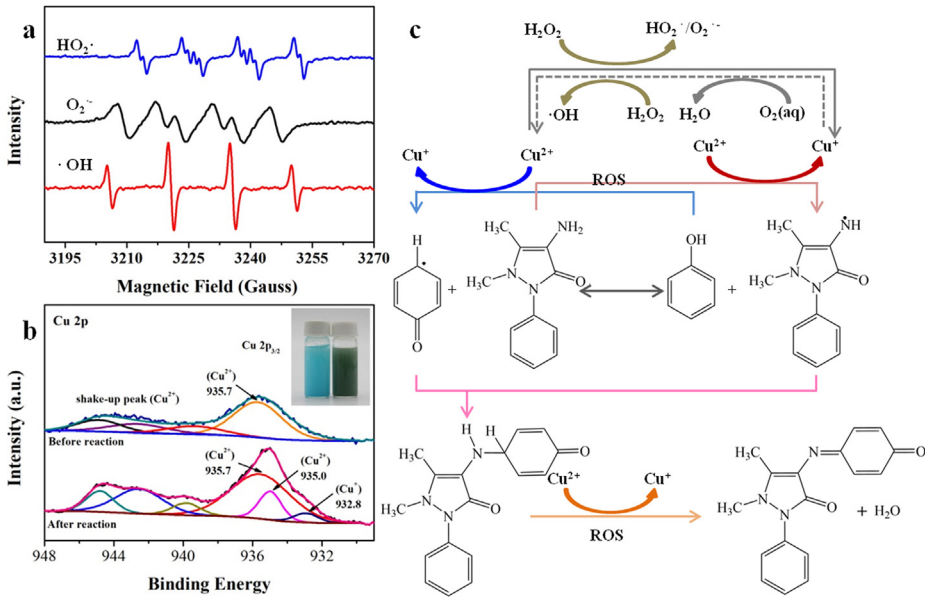

Fig. 3. (a) ESR spectra in Cu-NFs-2 system with the DMPO as a spin trap gent, (room temperature, 0.5 mg/mL Cu-NFs-2, 25 mM H_2O_2, 0.1 M pH 7.5 PB solution). (b) XPS spectra of the $Cu2p_{3/2}$ core levels of Cu-NFs-2 before and after the reaction of System 4#. (c) Reaction mechanism for dye formation.

$$Cu^{+} + H_2O_2 \rightarrow Cu^{2+} + \cdot OH + OH^{-} \quad (2)$$

$$HO_2^{\cdot} \rightarrow O_2^{\cdot -} + H^{+} \quad (3)$$

$$Cu^{+} + O_2(aq) \rightarrow Cu^{2+} + O_2^{\cdot -} \quad (4)$$

$$Cu^{+} + O_2(aq) + 4H^{+} \rightarrow 4Cu^{2+} + 2H_2O \quad (5)$$

The highly efficient oxidizing ROS produced in Eqs. (1)–(4) can catalyze the negatively charged phenoxy radical ions (PhO^{-}) to lose electrons to form phenoxy radicals ($PhO^{\bullet}$), while both of ROS and $PhO^{\bullet}$ can oxidize 4-AAP ($AmNH_2$) generates amino radicals ($AmNH^{\bullet}$) [49–51]. Simultaneously, the Cu^{2+} was also involved in the formation of $PhO^{\bullet}$ and $AmNH^{\bullet}$. Finally, the combination of $PhO^{\bullet}$ and $AmNH^{\bullet}$ in the presence of ROS and Cu^{2+} resulted in a co-oxidized product of pink antipyrilquinoneimine dye (Fig. 3c). The specific reaction equation is as follows:

$$PhOH \rightarrow PhO^{-} + H^{+} \quad (6)$$

$$PhO^{-} + Cu^{2+} \xrightarrow{ROS} PhO^{\cdot} + Cu^{+} \quad (7)$$

$$AmNH_2 + Cu^{2+} \xrightarrow{ROS} AmNH^{\cdot} + Cu^{+} \quad (8)$$

$$PhO^{\cdot} + AmNH_2 \rightarrow AmNH^{\cdot} + PhOH \quad (9)$$

$$PhO^{\cdot} + AmNH^{\cdot} \rightarrow Am - NH - OPh \quad (10)$$

$$Am - NH - OPh + Cu^{2+} \xrightarrow{ROS} Dye + Cu^{+} + H_2O \quad (11)$$

A total reaction equation is obtained as:

$$PhOH + AmNH_2 + H_2O_2 \xrightarrow{Cu^{2+}} Dye + 4H_2O \quad (12)$$

From the analysis results of the enzyme-like catalytic mechanism, it can be seen that the excellent catalytic activity of Cu-NFs-2 is not only due to its large specific surface area, but also to its abundant Cu^{2+} active sites on the surface of Cu-NFs-2. The Cu^{2+} active sites on the surface of Cu-NFs-2 are divided into two types, one is Cu^{2+} from the inorganic component of $Cu_3(PO_4)_2$ crystal. The $Cu_3(PO_4)_2$ crystal can quickly catalyze the decomposition of H_2O_2 to produce highly oxidative ROS under weak alkaline conditions. The other type is Cu^{2+} coordinated to the protein backbone during the initial growth of Cu-NFs-2. The coordinated Cu^{2+} has a chemical structure similar to that of natural polyphenol oxidase, so Cu-NFs-2 can also directly catalyze the coupling reaction between PhOH and 4-AAP in the absence of H_2O_2.

3.4. Reproducibility and stability of Cu-NFs-2

The biggest difference with natural enzymes is that Cu-NFs-2 is easily separated from the reaction solution. The relative activity of Cu-NFs-2 was calculated based on the absorbance (505 nm) of the first round reaction system as 100%. Fig. S9a shows that Cu-NFs-2 maintained 89.52% of the initial activity after repeating the reaction for 8 rounds. This demonstrates that Cu-NFs-2 possesses a good reproducibility in the catalytic process. The storage stability analysis is shown in Fig. S9b. The Cu-NFs-2 maintained more than 91.02% of its catalytic activity after one month of storage in PB solution (pH = 7.4) at room temperature, whereas the native HRP only retained about 46.72% of its initial activity. It is worth noting that repeated use and long-term storage have no significant effect on the morphology of Cu-NFs-2 (Fig. S9c and d), indicating that Cu-NFs-2 is highly stable in the chemical environment.

3.5. Characterization of Cu-NFs-2@Biotin-NHS-Ab_2 capture probes

Based on the excellent catalytic activity and good biocompatibility of Cu-NFs-2, it was selected as the carrier material for the immobilization of Ab_2. Avidin, an alkaline, obtained from CEW that can quickly and specifically bind to biotin. Avidin has a high affinity to biotin ($K_d \approx 10^{15}$ M), which is at least 10,000 times higher than that of antigens and antibodies. [52]. In this work, Ab_2 molecules were immobilized on the surface of Cu-NFs-2 by labeled avidin-biotin (LAB) method. The surface morphology, elements distribution and atomic percentage of elements the Cu-NFs-2@Biotin-NHS-Ab_2 capture probe were tested using Desktop SEM, TEM and EDS techniques, respectively. Fig. 4a2 shows the SEM image of Cu-NFs-2@Biotin-NHS-Ab_2 capture probes Cu-NFs-2@Biotin-NHS-Ab_2 capture probes. Compared with that of the bare Cu-NFs-2 (Fig. 4a1), the surface of the Cu-NFs-2@Biotin-NHS-Ab_2 capture

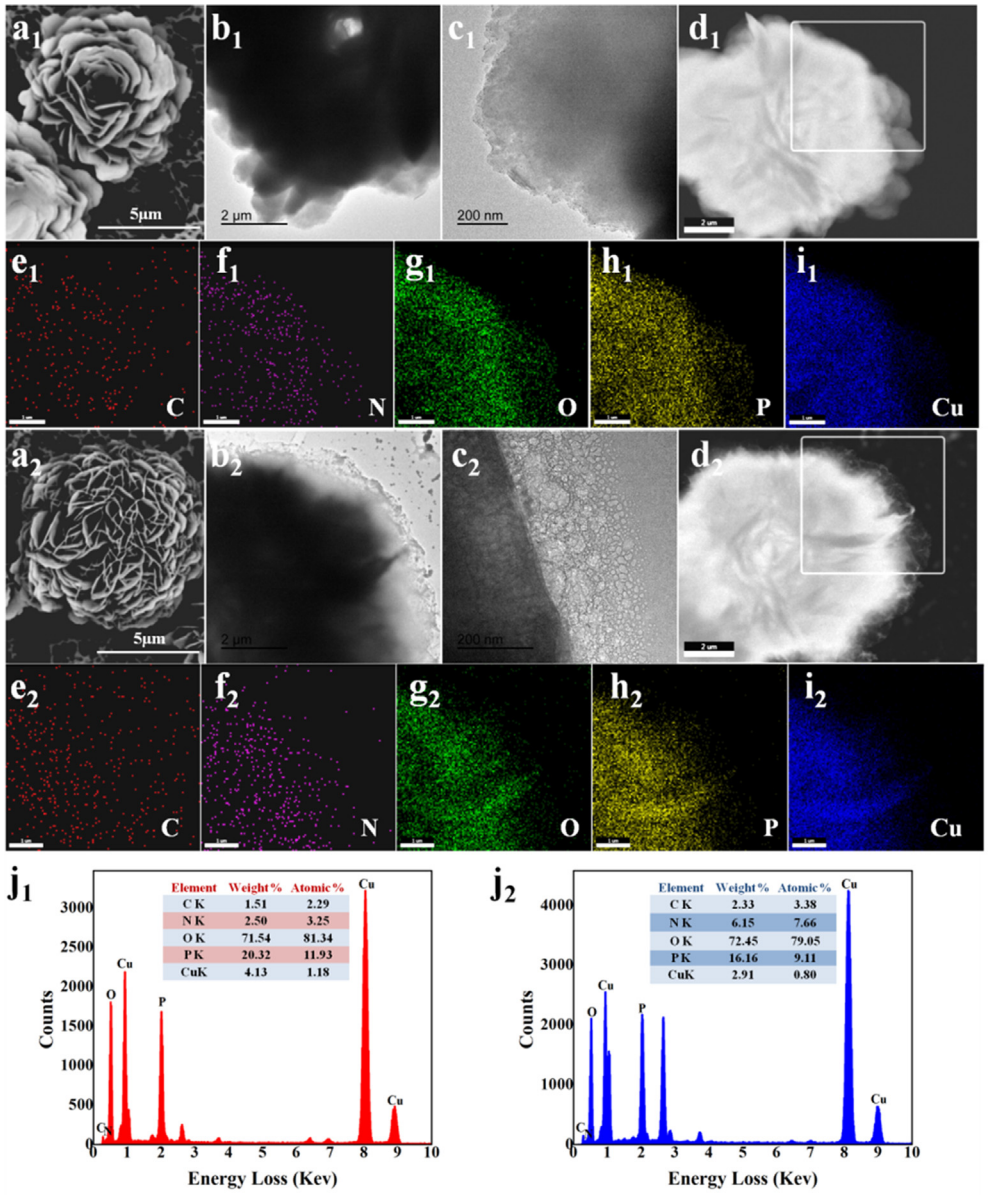

Fig. 4. Desktop SEM images (a), TEM images (b and c) and HAADF-STEM images (d) of the Cu-NFs-2 and Cu-NFs-2@Biotin-NHS-Ab_2 capture probes. (e-i) Element mapping images (C, N, O, P and Cu) according to (d). (j) EDS patterns of the Cu-NFs-2 and Cu-NFs-2@Biotin-NHS-Ab_2 capture probes. The images labeled 1 belong to the Cu-NFs-2 and labeled 2 belong to the Cu-NFs-2@Biotin-NHS-Ab_2 capture probes.

probe was covered with a layer of vine-like protein mesh. These protein meshes are Biotin-NHS-Ab_2 molecules. The Biotin-NHS-Ab_2 molecules denature, aggregate, and form an ordered protein network structure that may be caused by the gold spraying process performed by the sample before the SEM test. The TEM images of the partial nanoflower and nanopetals of Cu-NFs-2 were illustrated in Fig. 4b1 and c1. The prepared Cu-NFs-2 is composed of a large number of nanopetals pointing to the center of the microsphere, which is consistent with the SEM test results. For the TEM images of Cu-NFs-2@Biotin-NHS-Ab_2 capture probes (Fig. 4b2 and c2), it was clearly observed that the edges of the dark nanopetals were covered with a lighter protein coating [53]. The HAADF-STEM image (Fig. 4d) more vividly displays the geometric characteristics of Cu-NFs-2 and Cu-NFs-2@Biotin-NHS-Ab_2 capture probes. Fig. 4-e-i clearly shows that C, N, O, P and Cu elements are evenly distributed on the surface of the Cu-NFs-2 and Cu-NFs-2@Biotin-NHS-Ab_2 capture probes. By comparison, the content of N element on the surface of Cu-NFs-2@Biotin-NHS-Ab_2 capture probes increased significantly. The content change of N element on the surface of Cu-NFs-2 and Cu-NFs-2@Biotin-NHS-Ab_2 capture probes was further confirmed by EDS analysis. The weight percent and atomic percentage of N element increased from the original 2.50% and 3.25% to 6.15% and 7.66% (Fig. j), respectively. The above test results confirmed that the as-prepared Cu-NFs-2 possess specific biological recognition ability, and can effectively bind to biotin-labeled Ab_2 to fabricate a Cu-NFs-2@Biotin-NHS-Ab_2 capture probe.

3.6. Performance of the Cu-NFs-2-based LAB-ELISA for CEA assay

Combining the excellent efficiency catalytic activity and specificity capture CEA capability of the Cu-NFs-2@Biotin-NHS-Ab_2 capture probes, a Cu-NFs-2 based-LAB-ELISA colorimetric biosensor was established to realize the visualization and quantitative detec-

tion of CEA. As illustrated in Scheme 1, a typical sandwich ELISA method was applied in fabricating the colorimetric biosensor. First, the primary antibody (Ab_1) was adsorbed to the bottom of the 96-well plates and 1% BSA was used to prevent non-specific adsorption. Then CEA standards with different concentrations were added and bound strongly to Ab_1. Subsequently, the as-fabricated Cu-NFs-2@Biotin-NHS-Ab_2 capture probes, serving as the recognition unit, can capture CEA. After the sandwich immunoreactions, the System 5# solution was added to the processed 96-well plates. As a signal amplification unit, the Cu-NFs-2 can catalyze the oxidative coupling of PhOH and 4-AAP in the presence of H_2O_2 to produce a pink quinoneimine dye under weak alkaline (pH 7.5) conditions. Finally, the color variation of System 5# solution was observed by naked eyes and photographed, and then the absorbance (492 nm) of the System 5# solution was recorded by Microplate reader spectrophotometer. In the absence of the CEA, the as-fabricated Cu-NFs-2@Biotin-NHS-Ab_2 capture probes were washed away, resulting in a low background signal. Therefore, the concentration of CEA is determined only by visually observing the color variation or monitoring the absorbance intensities of System 5# solution. The CEA with different concentrations were detected by using Cu-NFs-2-based LAB-ELISA colorimetric biosensor. With the increasing of the CEA concentration, the color of the solution changed from colorless to pink colour, and the greater the concentration of CEA, the darker the color of solution (inset in Fig. 5). Subsequently, the absorbance at 492 nm of the solution with the concentration of CEA was further tested by microplate reader spectrophotometer, as shown in the Fig. 5. A linear relationship between absorbance and the logarithm of concentration (CEA) was observed in the range of 0.05–40 ng/mL. And the low detection limit (LOD) was estimated to be 3.52 pg/mL (S/N = 3). Compared with other reported strategies for CEA detection (Table S2), the as-developed colorimetric biosensor in this study exhibits a wider detection range and lower detection limit. It is particularly noteworthy that most of the reported nanoenzyme-based colorimetric sensor for CEA detection is performed under acidic conditions. Thus, the human **s**erum samples must be acidified before testing. This process not only complicates the operation, but also affects the accuracy of the test results. The as-developed colorimetric biosensor in this study effectively solves this problem and can detect CEA even at a pH value close to that of human serum.

3.7. Specificity and reliability of Cu-NFs-2-based LAB-ELISA for CEA

Four conventional human serum analytes including alpha-fetoprotein (AFP), immunoglobulin G (IgG), glucose (Glu), and ascorbic acid (AA) were used to evaluate the specificity of the developed Cu-NFs-2 based-LAB-ELISA colorimetric biosensor. As shown in the inset of Fig. S10, the color of the solution is pink colour only in the presence of CEA. Compared with the obvious absorbance response toward the target protein of CEA, no obvious absorbance responses were observed toward AFP, IgG, Glu and AA (Fig. S10), indicating excellent specificity of the developed colorimetric biosensor.

To evaluate the reliability of the developed colorimetric sensor for the analysis target, the detection of CEA in human serum sample was carried out. The human serum was diluted 100 times with 0.01 M pH 7.4 PBS before each experiment in order to diminish false positive contributions from the matrix. A series of human serum samples containing various CEA concentrations (0.05, 5, 20 and 40 ng/mL) were prepared by "spiking" them with a stock solution of CEA. Human serum samples display an obvious color change from colorless to pink with the increase of concentration of CEA (the inset of Fig. S11). According to the standard curve, the recovery of CEA in human serum samples was calculated between 97.0 and 106.0%, and the relative standard deviation (RSD) values was 0.76 ~ 2.12% (Table S3). These results reveal that the developed Cu-NFs-2 based-LAB-ELISA colorimetric biosensor has excellent reliability in real sample analysis. The excellent reliability of the developed colorimetric biosensor is related to the immunity experiment carried out under the environment of pH 7.5. The pH of healthy human serum is 7.35 ~ 7.45, which is very similar to the chemical environment of immunoassay.

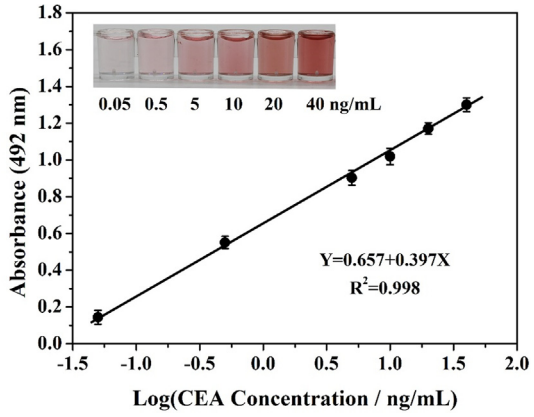

Fig. 5. Calibration plot of the Cu-NFs-2-based LAB-ELISA for determination of CEA standards; Inset: colorimetric responses of the sensing system in the presence of different concentration of CEA (0.05, 0.5, 5, 10, 20 and 40 ng/mL) (n = 16).

4. Conclusions

In summary, the dual-functional flower-like Cu-NFs has been synthesized by a one-pot method, and was used to construct a simple and convenient colorimetric biosensor for the detection of CEA. The as-prepared Cu-NFs possesses significantly improved physicochemical stability and a unique catalytic condition close to the human physiological environment, and its performance surpasses many natural enzymes and traditional nanoenzymes [16,17]. Compared with the previously reported method [15,54,55], the as-developed Cu-NFs-2 based-LAB-ELISA colorimetric biosensor exhibits superior performance for sensing CEA with a broad linear range from 0.05 to 40 ng/mL, low detection limit of 3.52 pg/mL, and high reproducibility, stability, specificity and reliability. Moreover, this colorimetric biosensor can visually detect the CEA (0–20 ng/mL) in human serum, which will be suitable for early cancer diagnosis in resource-poor health care institutions. At present, the as-developed colorimetric sensor realizes the detection of CEA through the change of the monochromatic intensity of the solution, which seriously confines the accuracy of visual detection. Therefore, the follow-up study will mainly focus on the design of Cu-NFs-based immunochromatographic test strips, which is expected to obtain a CEA analysis device with simple design, low cost and easy to read information.

CRediT authorship contribution statement

Jiaojiao Gao: Conceptualization, Methodology, Validation, Investigation, Formal analysis, Writing - original draft. **Hui Liu:** Conceptualization, Methodology, Validation, Formal analysis, Writing - review & editing, Visualization, Supervision. **Kexin Wu:** Resources, Investigation, Data curation. **Jifeng Yan:** Resources, Investigation, Data curation. **Huayu Li:** Resources, Investigation, Data curation. **Ruixuan Yang:** Resources, Investigation, Data curation. **Cheng Tong:** Visualization. **Lingyan Pang:** Writing - review & editing. **Junqi Li:** Writing - review & editing.

Declaration of Competing Interest

The authors declare that they have no known competing financial interests or personal relationships that could have appeared to influence the work reported in this paper.

Acknowledgments

We acknowledge the financial support from the National Science Foundation of China (51272147), the Natural Science Foundation of Shaanxi Province (2015JM5208), the Foundation for Young Scholars of Shaanxi University of Science &Technology (no. 2017BJ-06), the Natural Science Foundation of Shaanxi Province (no. 2018JQ2069), and the Graduate Innovation Found of Shaanxi University of Science & Technology.

Appendix A. Supplementary data

Supplementary data to this article can be found online at https://doi.org/10.1016/j.jcis.2021.05.069.

References

[1] B. Freddie, F. Jacques, S. Isabelle, S. Rebecca, A.T. Lindsey, J. Ahmedin, Ca-Cancer J. Clin. 68 (2018) 394.
[2] J. Ferlay, M. Colombet, I. Soerjomataram, C. Mathers, D.M. Parkin, M. Piñeros, A. Znaor, F. Bray, Int. J. Cancer 144 (2019) 1941.
[3] A. Dubecz, I. Gall, N. Solymosi, M. Schweigert, J.H. Peters, M. Feith, H.J. Stein, J. Thorac. Oncol. 7 (2012) 443.
[4] R.S. Herbst, D. Morgensztern, C. Boshoff, Nature 553 (2018) 446.
[5] L. Harris, H. Fritsche, R. Mennel, L. Norton, P. Ravdin, S. Taube, M.R. Somerfield, D.F. Hayes, R.C. Bast, J. Clin. Oncol. 25 (2007) 5287.
[6] C.C. Woo, E.G. Se, Ann. Oncol.: Off. J. Eur. Soc. Med. Oncol. 28 (2017) 36.
[7] J.M. Lee, M.-H. Lee, E. Garon, J.W. Goldman, R. Salehi-Rad, F.E. Baratelli, D. Schaue, G. Wang, F. Rosen, J. Yanagawa, T.C. Walser, Y. Lin, S.J. Park, S. Adams, F. M. Marincola, P.C. Tumeh, F. Abtin, R. Suh, K.L. Reckamp, G. Lee, W.D. Wallace, S. Lee, G. Zeng, D.A. Elashoff, S. Sharma, S.M. Dubinett, Clin. Cancer Res. 23 (2017) 4556.
[8] Y. Xie, M. Zhang, Q. Bin, S. Xie, L. Guo, F. Cheng, W. Lv, Biosens. Bioelectron. 150 (2020) 111949.
[9] Z. Qiu, J. Shu, D. Tang, Anal. Chem. 89 (2017) 5152.
[10] H. Tang, J. Chen, L. Nie, Y. Kuang, S. Yao, Biosens. Bioelectron. 22 (2007) 1061.
[11] Z. Guo, T. Hao, S. Du, B. Chen, Z. Wang, X. Li, S. Wang, Biosens. Bioelectron. 44 (2013) 101.
[12] J. Peng, Y. Lai, Y. Chen, J. Xu, L. Sun, J. Weng, Small 13 (2017) 1.
[13] A.V.S. Piriya, P. Joseph, K.S.C.G. Daniel, S. Lakshmanan, T. Kinoshita, S. Muthusamy, Mater. Sci. Eng., C 78 (2017) 1231.
[14] Y. Liu, J. Chen, M. Du, X. Wang, X. Ji, Z. He, Biosens. Bioelectron. 92 (2017) 68.
[15] Y. Yao, W. Guo, J. Zhang, Y. Wu, W. Fu, T. Liu, X. Wu, H. Wang, X. Gong, X.J. Liang, ACS Appl. Mater. Interfaces 8 (2016) 22963.
[16] X. Liu, D. Huang, C. Lai, L. Qin, G. Zeng, P. Xu, B. Li, H. Yi, M. Zhang, Small 15 (2019) 1900133.
[17] L. Gao, J. Zhuang, L. Nie, J. Zhang, Y. Zhang, N. Gu, T. Wang, J. Feng, D. Yang, S. Perrett, Nat. Nanotechnol. 2 (2007) 577.
[18] H. Wei, E. Wang, Anal. Chem. 80 (2008) 2250.
[19] S. Chen, X. Hai, X.W. Chen, J.H. Wang, Anal. Chem. 86 (2014) 6689.
[20] J. Ge, J. Lei, R.N. Zare, Nat. Nanotechnol. 7 (2012) 428.
[21] J. Cui, S. Jia, Coord. Chem. Rev. 352 (2017) 249.
[22] X. Zhang, Y. Ding, H. Tang, X. Han, N. Wang, Chem. Eng. J. 236 (2014) 251.
[23] L. Zhang, Y. Nie, C. Hu, J. Qu, Appl. Catal., B 125 (2012) 418.
[24] L. Sun, H. Song, Q. Li, A. Li, Chem. Eng. J. 283 (2016) 366.
[25] J. Gao, H. Liu, L. Pang, K. Guo, J. Li, ACS Appl. Mater. Interfaces 10 (2018) 30441.
[26] A.T. Marttila, O.H. Laitinen, K.J. Airenne, T. Kulik, M.S. Kulomaa, FEBS Lett. 467 (2000) 31.
[27] C. Guérin-Dubiard, M. Pasco, D. Mollé, C. Désert, T. Croguennec, F. Nau, J. Agric. Food Chem. 54 (2006) 3901.
[28] R. Jin, D. Kong, X. Zhao, H. Li, X. Yan, F. Liu, P. Sun, D. Du, Y. Lin, G. Lu, Biosens. Bioelectron. 141 (2019) 111473.
[29] H. Shao, N. Padmanathan, D. McNulty, C. O'Dwyer, K.M. Razeeb, ACS Appl. Mater. Interfaces 8 (2016) 28592.
[30] M. Weber, F.C. Nart, Electrochim. Acta 41 (1996) 653.
[31] S.K.S. Patel, H. Choi, J.K. Lee, ACS Sustainable Chem. Eng. 7 (2019) 13633.
[32] L. Tian, W. Zhao, L. Li, Y. Tong, G. Peng, Y. Li, Sens. Actuators, B 240 (2017) 114.
[33] T.M. Ivanova, K.I. Maslakov, A.A. Sidorov, M.A. Kiskin, I.L. Eremenko, J. Electron Spectrosc. Relat. Phenom. 238 (2020) 146878.
[34] W. Zhang, A. Sun, X. Zhao, X. Pan, Y. Han, N. Suo, L. Yu, Z. Zuo, J. Alloys Compd. 816 (2020) 152501.
[35] Y. Zhang, J. He, Z. Gao, X. Li, Nano Energy 65 (2019) 104045.
[36] M.K. Kumar, J.Y. Do, S.V.P. Vattikuti, P.A.K. Reddy, M. Kang, J. Alloys Compd. 750 (2018) 292.
[37] S.M. Alshehri, A.N. Alhabarah, J. Ahmed, M. Naushad, T. Ahamad, J. Colloid Interface Sci. 514 (2018) 1.
[38] J. Chang, Z. Gao, X. Liu, D. Wu, F. Xu, Y. Guo, K. Jiang, Electrochim. Acta 213 (2016) 382.
[39] X. Xu, J. Zou, X.R. Zhao, X.Y. Jiang, F.P. Jiao, J.G. Yu, Q. Liu, J. Teng, Colloids Surf., A 570 (2019) 127.
[40] X. Liu, W. Hu, S. Yang, Z. Li, C. Pei, Y. Zhou, G. Yin, Corros. Sci. 94 (2015) 270.
[41] Z. Zeng, L. Tian, Z. Li, L. Jia, X. Zhang, M. Xia, Y. Hu, Biosens. Bioelectron. 69 (2015) 162.
[42] H.Y. Kim, H.J. Lee, S.K. Chang, Talanta 132 (2015) 625.
[43] Z. Lin, Y. Xiao, Y. Yin, W. Hu, W. Liu, H. Yang, ACS Appl. Mater. Interfaces 6 (2012) 10775.
[44] Y. Wang, Y. Liu, Y. Liu, Chem. Eng. J. 372 (2019) 92.
[45] Q. Zhang, C. Zhang, S.A. Shahzad, C. Yu, Talanta 158 (2016) 342.
[46] F. Chen, X. Zhao, H. Liu, J. Qu, Appl. Catal., B 158 (2014) 85.
[47] O. Fueman, D.F. Laine, A. Blumenfeld, A.L. Teel, K. Shimizu, I.F. Cheng, R.J. Watts, Environ. Sci. Technol. 43 (2009) 1528.
[48] R. Hu, Y. Fang, M. Huo, H. Yao, C. Wang, Y. Chen, R. Wu, Biomaterials 206 (2019) 101.
[49] M. Kidwai, A. Jain, A. Sharma, R.C. Kuhad, Water Sci. Technol. 66 (2012) 385.
[50] A. Córdoba, N. Alasino, M. Asteasuain, I. Magario, M.L. Ferreira, Chem. Eng. Sci. 129 (2015) 249.
[51] N.R. Curvetto, D. Figlas, A. Brandolin, S.B. Saidman, E.H. Rueda, M.L. Ferreira, Biochem. Eng. J. 29 (2006) 191.
[52] V.P. Hytönen, H.R. Nordlund, J. Hörhä, T.K.M. Nyholm, D.E. Hyre, T. Kulomaa, E. J. Porkka, A.T. Marttila, P.S. Stayton, O.H. Laitinen, M.S. Kulomaa, Proteins 61 (2010) 597.
[53] J. Yan, Y. Liu, Y. Wang, X. Xu, Y. Lu, Y. Pan, F. Guo, D. Shi, Sens. Actuators, B 197 (2014) 129.
[54] N. Alizadeh, A. Salimi, R. Hallaj, Talanta 189 (2018) 100.
[55] Y. Jia, B. Zhang, H. Chang, F. Yu, Z. Zhao, J. Pharm. Biomed. Anal. 169 (2019) 75.